Int. J. Electrochem. Sci., 14 **(2019)** 1024 – 1039, doi: 10.20964/2019.01.93

International Journal of ELECTROCHEMICAL SCIENCE
www.electrochemsci.org

Study on the Under-Rib Convection for Improving *in situ* Reactants Supply and Water Discharge, hysteresis effect and Current Density Distributions for Polymer Electrolyte Fuel Cells

Hyung-Man Kim[*]

Department of Mechanical Engineering & High Safety Vehicle Core Technology Research Center, INJE University, 607 Eobang-dong, Gimhae-si, Gyongsangnam-do 621-749, Republic of Korea
[*]E-mail: mechkhm@inje.ac.kr

Received: 31 July 2018 / *Accepted:* 16 October 2018 / *Published:* 30 November 2018

New flow-field design with the under-rib convection (URC) aims to enhance polymer electrolyte fuel cell (PEFC) performance. This paper presents the experimental and numerical results for single cells with a new flow-field that stimulates URC with additional sub-channels and by-passes to a conventional flow-field with 5-passes and 4-turns on an active area of 25 cm^2. To characterize the role of under-rib convection for PEFC's polarization performance, the performance related parameters of *in situ* reactants and liquid water flows, hysteresis effects and current density distributions of a new serpentine flow-field with sub-channels and by-passes (SFFSB) were compared experimentally and numerically with those of conventional SFFs without SB (CASFF). Hysteresis curves of the new SFFSB design featured a considerably smaller area than those of the CASFF design, because hysteresis curves measure variation of polarization by electric load. The hysteresis effects of PEFCs were investigated between the SFF without and with sub-channels and by-passes (SBs) designs. In the single cell of a CASSF, the areas of hysteresis loops over five cycles were evaluated statistically, obtaining a polarization curve of 0.03836 $\pm$ 0.001431 (mean $\pm$ s.e.m.) and a power density curve of 0.02889 $\pm$ 0.002181. In the single cell of the new SFFSB, the area of hysteresis loops over five cycles was measured variation of polarization by electric load, obtaining a polarization curve of 0.03581 $\pm$ 0.0006720 and a power density curve of 0.02307 $\pm$ 0.0005538. In the experimental measurement of PEFC polarization curve, the average current density of the new SFFSB, 1.557 A/cm^2, was increased by 18.85% compared to that of the CASFF, 1.310 A/cm^2 at a cell's voltage of 0.35 V; the maximum power densities of the SFFSB and CASFF were 0.615 and 0.497 W/cm^2 at a cell's voltage of 0.47 V, respectively, demonstrating an improvement of 23.74% in the new SFFSB. The current density distribution verified the PEFC's performance improved by URC with the new SFFSB. The new SFFSB was determined to realize more balanced reactants concentration distribution from inlet to outlet and to activate the electrochemical reaction by increasing mass transport rates of reactants from flow channel to inner catalyst layer and by facilitating liquid water removal from URC regions. URC will play a significant role in improving PEFC's performance, furthermore, increasing the fuel cell lifetime.

Keywords: Polymer electrolyte fuel cell; Serpentine flow-field; Under-rib convection; Maximum performance test; Current density distribution

1. INTRODUCTION

Polymer Electrolyte Fuel Cells (PEFCs) fueled with hydrogen are among the most prospective energy conversion technologies for the broadest of applications, including portable, stationary and automotive power delivery [1]. One of the main obstacles to the commercialization of PEFCs is the flow-fields in the bipolar plate (BP) that causes severe water flooding and mass transport loss of the cathode. Nevertheless, the bipolar plate (BP) design and the flow channel layout configuration particularly have the potentiality to make an alternative clean energy source compatible with its counterparts [2].

In principle, channel structure offers the homogeneous flow distribution with low-pressure drops. However, the formation of liquid water at the cathode can flood channels as a consequence of interrupting the gas flow there. To efficiently use the area, the flow distribution should be as homogeneous as possible [3]. Because the saturated vapor pressure of water exponentially increases with cell's temperature, there is an optimal temperature window for maximizing performance. Too high flow stoichiometry causes cell's dry-out, while too low flow stoichiometry causes the oxygen partial pressure that is too low and mass transport losses [4]. Under-rib convection (URC) is increasingly important above 10^{-13} m^2 of the gas diffusion layer (GDL) permeability; this result is consistent with the numerical expectation of the relative influence of URC [5,6]. The mass transfer in a PEFC can be considered as the mass transport phenomenon between the electrodes and the flow-field because of both diffusion and convection that are influenced by the flow-field transfiguration because the optimization of mass transfer can reduce the concentration loss. The selection of the flow-field pattern is important because of the effect that the shape, size and pattern of the corresponding flow-field have on PEFC's polarization performance.

An improvement in the performance of PEFCs as well as direct methanol fuel cells (DMFCs) is attract to many researchers who have focused on flow-field design, both by numerical simulation and by experimental approach [7-17]. In the research early stage on flow-field development, cross convection has been widely neglected. In the first few studies to address this effect, two borderline cases for a serpentine flow-field were observed: one in which all the fluids follow the channel; one where all the fluid passes through the GDL. The latter reduces the pressure drop in flow channel. PEFC with serpentine flow channels of a square cross-section were numerically investigated to understand well the influence of channel-to-channel gas crossover on pressure and temperature distributions [7]. DMFC with various flow-field patterns was experimentally studied on the reduction of cell's performance; as a consequence of thinning the backing layer, may be attributed primarily to increase under-rib convection-driven mass transport polarization [8]. PEFC with serpentine-baffle flow-field was numerically studied; as a consequence, the baffled design increases the limiting current density and improves the cell's performance relative to conventional design [9]. PEFC with single serpentine flow-field (SFF) was numerically studied; low channel heights improve URC to transport oxygen and liquid water out of the diffusion layer [10]. PEFC with multi-pass serpentine flow-fields was numerically studied; as a result, multi-pass serpentine flow-fields lead to significantly high URC intensities [11]. The convection

transport mechanism has been referred to as convection through the GDL, channel-to-channel gas crossover, cross-leakage flow and sub-rib convection. URC has recently been recognized as a non-negligible transport process that affects the performance of PEFCs and DMFCs as a result of the higher GDL permeability.

In previous studies, a systematic design process was developed for the SFF to enhance the PEFC's performance through detailed parametric studies. PEFC with the new SFFSB has been numerically developed the promotion method of URC [12-15,17] and the enhancement of the PEFC's polarization performance was experimentally verified by utilizing H_2/air and H_2/O_2 with 15 W and 60 W class single cell with an active areas of 25 cm^2 and 100 cm^2, respectively, and 60 W and 1 kW class 4-cell and 20-cell stacks with active areas of 25 cm^2 and 150 cm^2, respectively [15-18]. These results increase understanding and utilization of under-rib convective flow. Reactants flow in the same direction as the neighboring main channels, the under-rib convective flows converged from the main channels into the sub-channels, not only reducing the pressure drop but also enhancing the uniform gas supply and water discharge. The maximum current and power densities of the SFFSB were increased suddenly due to the promotion of URC. It is necessary to minimize the activation loss region, the ohmic resistance loss region and the mass transport loss region. It is understood that the flow-field design plays a significantly important role in mass transfer and water management; therefore, great efforts have been made to achieve an optimized design of the flow-field that would guarantee high and stable cell's polarization performance. It is desirable for PEFC to be operated at a uniform current density over the membrane electrode assembly (MEA) because unbalanced current distribution in a PEFC could results in poor reactants and electrocatalyst utilization, low energy efficiency, and possible corrosion inside the fuel cell. Local current distribution in PEFC can be significantly affected both by the operating conditions and by the optimization of the reactants flow arrangement between anode and cathode streams, especially in the commercialization of PEFCs with large cell sizes.

In this study, the proposed URC mechanism are investigated the effects on the enhancement of reactants uniformity, water balance, electrochemical reaction, hysteresis of polarization, and power density and current density distribution by comparing the SFFSB to promote URC with the CASFF. PEFC's polarization performance is determined by measuring the polarization and power density curves and their hysteresis while adjusting the operating conditions such as pressure, temperature, humidity, flowrate and reactants. To characterize the hysteresis effects of PEFC's polarization performance for dynamic operation, detailed data related to the effects of hysteresis on the polarization and power densities are presented. Furthermore, the *in situ* current density distribution is directly measured to present the proposed URC mechanism and the effects on the uniformity of the current density are evaluated by electrochemical reaction. The growth of the water flooding phenomenon has been confirmed as approaching the anode outlet; the relationship with mass transport loss can cause the degradation of PEFC's polarization performance in a flooding phenomenon. Maximum performance tests are performed to confirm the numerical analysis and the uniformities of current density distributions are evaluated experimentally based on the mass transfer mechanism of the numerical analysis using the PEFC test station which measures *in situ* current density distribution at the activation loss region, the ohmic resistance loss region and the mass transport loss region, respectively.

2. NUMERICAL ANALYSIS-BASED DESIGN OF THE SFF WITH SBs

Three-dimensional Fully coupled electrochemical model equations were solved using the commercial computational fluid dynamics (CFD) software based on STAR-CD version 4.12, a commercial finite volume technique solver and ES-PEMFC version 2.40, an add-on tool modulated for PEFCs. The numerical assumptions are steady state, ideal gas properties and homogeneous two-phase flows. The numerical modeling is based on a single domain formulation. The conservation equations are solved for mass, momentum, species, energy and charge with electrochemical reactions. Assuming that liquid film is formed on the electrode surface during liquid water condensation, Henry's law of solubility of gases in liquid water is used to calculate the diffusion flux, electro-osmotic drag force, and water back diffusion and etc. [12-15].

To enhance the computational accuracy, grid cells were established by equalizing the node connectivity in each component and by using the hexahedron mesh. The present numerical model was verified by grid tests and the results of numerical simulation on PEFCs [19]. The convergence criteria for the mass balance and energy balance are 1% with the maximum residual tolerance of 1E-07.

Through the previous geometrical optimization of SFFs with various heights and widths of channel and rib, numerical analysis-based design for optimum SFF of 5-passes and 4-turns on an active area of 25 cm^2 were considered as a standard flow-field in this study [18]. To stimulate URC, SFFSB were optimized to improve PEFC's polarization performance [13]. Figure 1 shows two 25 cm^2 serpentine flow-fields without and with SBs of 5-passes and 4-turns, and Table 1 lists the geometric parameters considered in this study.

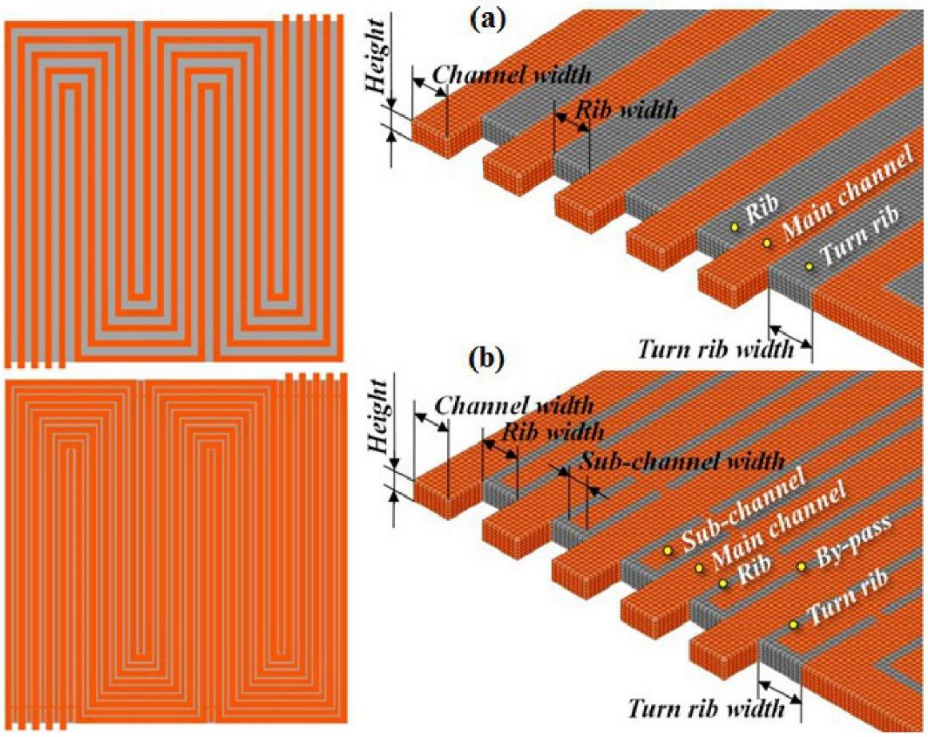

Figure 1. Schematics of the two SFF patterns of 5-passes and 4-turns on an active area of 25 cm^2; (a) without SBs, (b) with SBs [adapted from Ref. 13].

Table 1. Operating conditions and geometrical details of two flow-fields used in this study [12].

Inlet conditions	**Anode**	**Cathode**
Gas	Hydrogen	Air
Stoichiometry	1.5	2.0
Inlet temperature (℃)	70	70
Inlet relative humidity (%)	100	100
Mass fraction of Hydrogen	0.078	-
Mass fraction of Oxygen	-	0.169
Mass fraction of Water	0.561	0.274
Operating conditions		
Exit pressure (kPa)	101	
Open circuit voltage (V)	0.96	
Cell temperature (℃)	70	
SFF patterns	**w/o SBs**	**w/ SBs**
Main channel width (mm)	1.0	1.0
Main channel rib width (mm)	1.0	1.0
Main channel turn rib width (mm)	1.25	1.25
Main channel height (mm)	0.5	0.5
Sub-channel width (mm)	-	0.5
Sub-channel turn rib width (mm)	-	0.75
Sub-channel height (mm)	-	0.334
By-pass width (mm)	-	0.25
By-pass height (mm)	-	0.334
Cross-sectional area (cm^2)	0.025	0.025

3. EXPERIMENTAL PROCEDURE

In electrochemical experiments, basic three variables of voltage (V), current (*I*) and time (*t*) must be measured. Due to the mutual dependence between voltage (V) and current (*I*), the both variables cannot be changed independently at the same time. Therefore, they are measured with potentiostatic technique and galvanostatic technique. Since the performance of fuel cell is greatly depending on operating conditions, the operating pressure, temperature, humidity, flow rate, and reacting gas must be freely adjustable. Reacting gases such as hydrogen and oxygen must be carefully moved from the container to the entrance of fuel cell without any changes of temperature, pressure and flow rate. The PEFC's performance is greatly affected by temperature, pressure, flow rate, and humidity [14]. Thus, the custom designed test equipment was constructed with flow direction controller, flow controller, temperature controller, humidity sensor module, mass flow controller and read out unit, electronic load, power supply module, and data acquisition system to control the operational condition of fuel cell

continuously. Specification and structure of each device are as following: Electronic load (KIKUSUI PLZ-664WA); Flow controller system; Temperature controller; Relative humidity sensor (VAISALA HMT337); Data acquisition system (DEWETRON DEWE-30-16).

To measure the current density distribution of fuel cell, the current scan lin developed by S^{++} Company was used to add sensor plates of 49 segments in the back of cathode separation plate as shown in Figure 2. Graphite foil was added to the contact side of current collector, sensor plate, and bipolar plate keeping contact areas and electrical conductivity the same to minimize any possible errors in the contract plates while measuring current density distribution.

Reactants of hydrogen and air must be carefully supplied from storage to the entrance of the PEFC because the PEFC's performance is influenced by operating conditions including temperature, pressure, flow rate, and humidity. Therefore, the custom built-in test equipment was equipped with a flow direction controller, flow controller, temperature controller, humidity sensor module, mass flow controller, electronic load, power supply module, and data acquisition system to continuously control the operational conditions of PEFC.

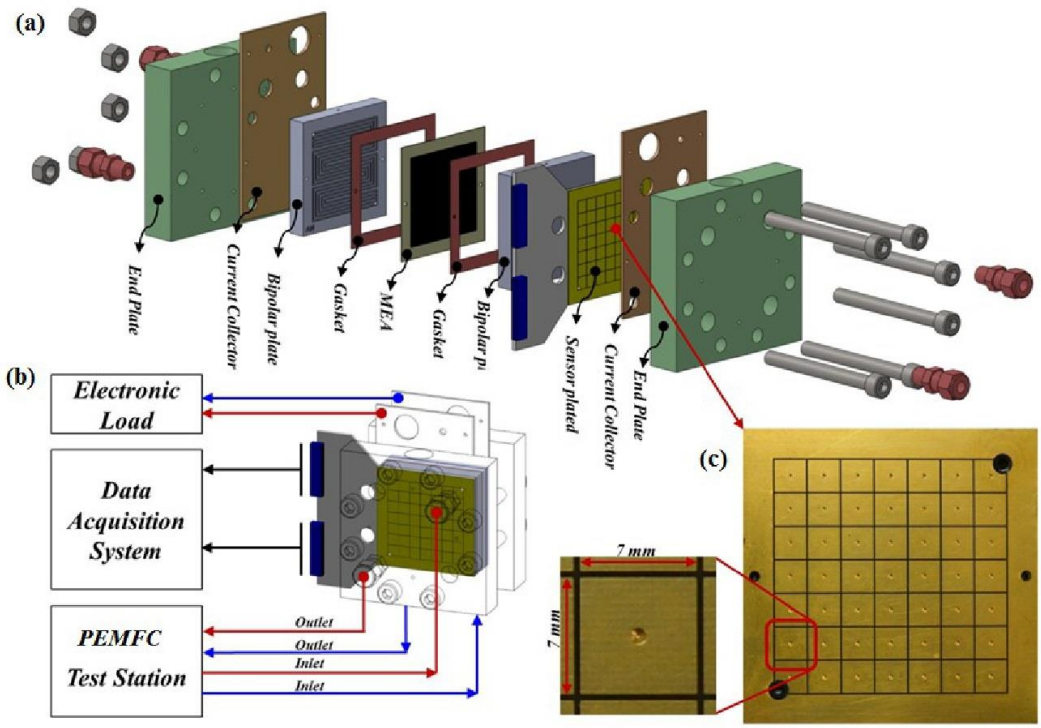

Figure 2. Experimental apparatus for measuring the *in situ* current density distribution with two SFF patterns of 5-passes and 4-turns on an active area of 25 cm^2: (a) schematic diagram of the incorporation of the current density sensor plate into a single PEFC; (b) interconnection block diagram around the current density sensor plate with PEFC test station instruments, a data acquisition system and an electronic load; (c) photograph of the current density sensor plate with segment positions [adapted from Ref. 15].

The segmented BP experiment was adapted to measure the local current density distribution in single PEFCs. The sensor plate, running a current scan Lin made by S++®, was used to measure the current density distribution. The measurement principle base is the dependence of the permeability of a magnetically soft material on magnetization and temperature [21].

4. RESULTS AND DISCUSSION

4.1. Numerical results of the role of URC in reactants and liquid water flows

Numerical analyses were studied on the bipolar plates of PEFC that have two 25 cm^2 with CASFF and SFFSB patterns; all the studies were conducted under the same operating conditions, as listed in Table 1. The numerical results of the CASFF patterns with optimized height and width were compared with those of the SFFSB patterns for promoting URC [13,18]. PEFC's polarization performance was analyzed using the present numerical model of mass transfer and electrochemical reaction that are three-dimensional fully coupled electrochemical model equations. As a consequence, the distributions of performance related parameters including the hydrogen and oxygen mass fraction, membrane water content, net water flux per proton, liquid water mass fraction, total pressure, temperature, current density, and polarization and power density curves are analyze in detail. The performance-related parameters are investigated to generate the optimal SFFSB that enhances PEFC polarization performance.

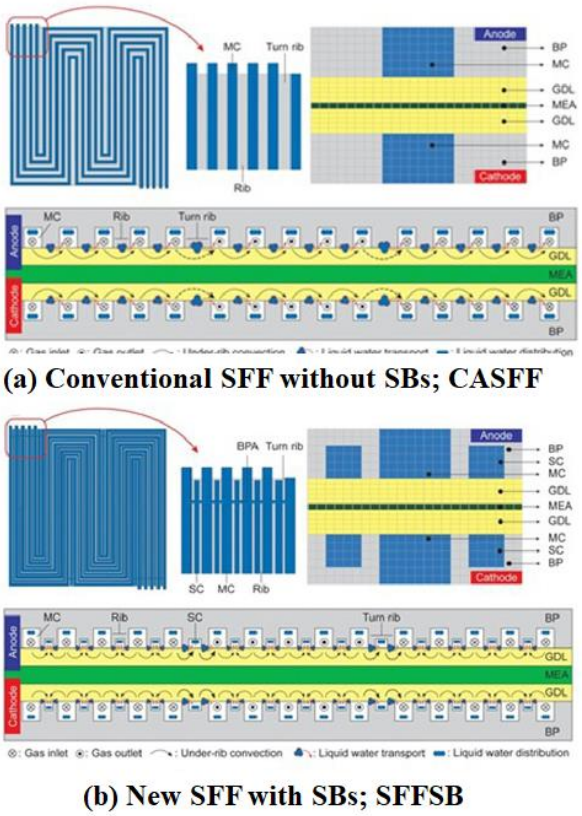

Figure 3. Schematics of the SFF (a) without SBs and (b) with SBs of 5-passes and 4-turns on an active area of 25 cm^2 and simulation results of the cross sectional views illustrating the typical reactants flow direction and liquid water transport caused by under-rib convection.

To verify URC's effects, figure 3 presents sectional views illustrating the typical reactants flow direction and liquid water transport driven by URC through the numerical results of flow direction and velocity vectors shown between CASFF and SFFSB of 5-passes and 4-turns on an active area of 25 cm^2 [12]. URC is additional convective flow through the GDLs that are designed to increase the mass transfer rates of the reactants from the flow channel to inside catalyst layer (CL) in order to realize more effective utilization of electrocatalysts by increasing reactants' concentration and improving liquid water removal into URC regions.

In the anode side of the CASFF shown in Fig. 3a, almost uniform velocity vectors can be observed in the main channel and rib area, presenting the same gas flow direction, but it shows a minor change from inlet to outlet direction. In the turn rib regions that provide a change in flow direction, the velocity vectors are significantly lifted due to the large pressure difference between adjacent main channels. Additionally, in the cathode side, URC is generated from inlet to outlet due to the high stoichiometry ratio, and high velocity vectors of SFFSB are observed in the adjacent rib and turn-rib regions.

However, in the case of SFFSB shown in Fig. 3b, rib width decreased; therefore, gas permeability and overall gas diffusion force are improved by additional sub-channels to change the flow direction of URC. Therefore, in the anode side of SFFSB, the velocity vectors increase inside the main channel inlet and the URC flow direction converges to a sub-channel through convection because the pressure of the main channel is higher than the sub-channel. The velocity vectors become uniform in the main channel outlet because of the pressure decrease. In cathode side, URC, with a different size but a similar tendency compared with the anode side is generated, and the flow direction of the URC is changed from the sub-channel to the main channel at the channel outlet because of the high stoichiometry ratio. This is because the internal pressure of the sub-channel is increased as the reactants, travelling through the sub-channel, moves to outlet, so the flow direction is changed toward the main channel for a smooth discharge.

Figure 3 illustrates the URC verifying mechanism of the flow direction and the liquid water transport of the SFFSB. The enhancement of URC can reduce water flooding at the cathode and increases the electrochemical reaction, thereby improving both PEFC polarization performance and durability.

4.2. Experimental results of the role of URC in hysteresis effects

For performance evaluation of fuel cell, CASFF and SFFSB models with 25cm^2 reaction area of 5-passes and 4-turns serpentine flow field were examined with activation test and performance test, and current density distribution was evaluated. CASFF and SFFSB were used in performance evaluation. The separation plates of anode and cathode were produced with semi-counter flow of reaction gas in the same format. MEA (membrane electrode assembly) and GDL (gas diffusion layer) used in the experiment were made of W.L. Gore & Associates PRIMEA® SERIES 57 MEA (anode: Pt catalyst 0.4 mg/cm^2, cathode: Pt catalyst 0.4 mg/cm^2) and SIGRACET® GDL 10 BC. To evaluate the performance and hysteresis of PEFCs, we fabricated two single cells on an active area of 25 cm^2 SFFs without and with SBs of 5-passes and 4-turns.

PEFC polarization performance was evaluated by the polarization curve measured while adjusting the pressure, temperature, humidity, and flow rate of the reacting gas using the test station [18].

We tested the polarization and power density of the two single cells over 5 cycles while the load currents were controlled according to predefined schedules.

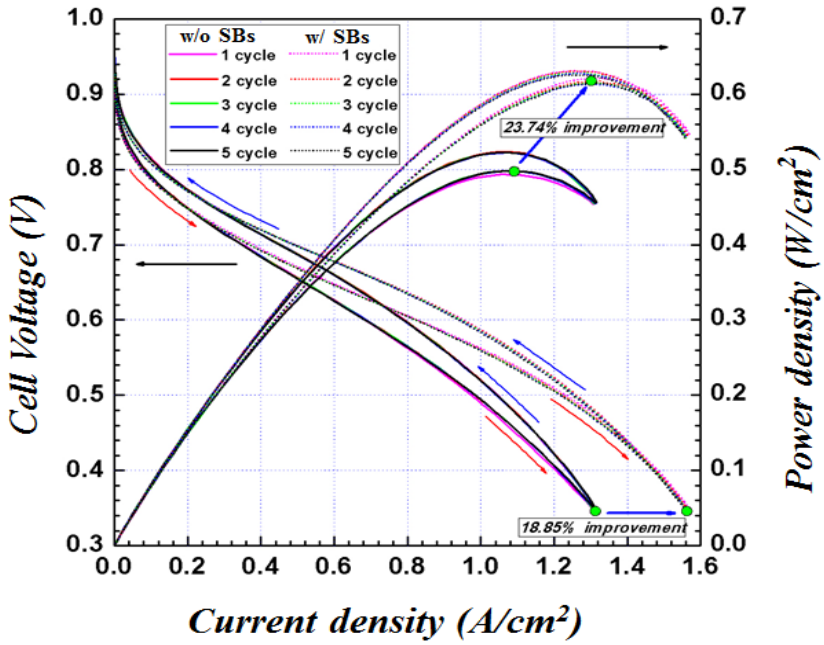

Figure 4. Experimental results of the polarization and power density hysteresis curves of the SFFs (a) without SBs and (b) with SBs under the operating conditions of stoichiometry of 1.5 H_2 on the anode/2.0 air on the cathode, a cell temperature of 70℃ and an inlet relative humidity of 100% RH.

Although the polarization and power density curves in the SFFs without and with SBs over 5 cycles were slightly different, such reproducible results were attributed to the change in the membrane conductivity, causing the water content to move towards a higher current density zone [23-24].

As shown in Fig. 4, the hysteresis of polarization curves can be shown during the repetitive increase and decrease of input current. The lower curves of hysteresis loops are created during increase of the input current, and the upper curves are created during decrease of the input current; these phenomena are related to the flooding and drying of the fuel cell, respectively. When flooding occurs on the cathode side, then operation at a higher current would only make worse due to additional water would be discharged. The polarization curve recorded under a decreasing current would represent lower voltage at higher currents than the polarization curve recorded under an increasing current [18]. These single cells experience some loss of efficiency and power density due to the scale up in the area of the electrodes and the increased number of cells in the stack. These maldistribution problems could be reduced if the manifold of a parallel gas distribution system was optimized to homogenize the gas distribution within the stack [25]. Recently, the convection-improved SFF design has been confirmed to exhibit a better water-handling ability than the conventional design [12-13,15], and the cathode flow-field design for PEFC with the new SFFSB promote strong convection flows to increase mass transport rates of reactants from flow channel to inner catalyst layer and more effective utilization of electrocatalysts by increasing reactants concentration and facilitating liquid water discharge [26].

Figure 4 shows the comparison of the polarization and power density curves over five cycles

between the single cells of the CASFF and the SFFSB for improving hysteresis. In the single cell of the CASFF, the areas of hysteresis loops over five cycles were compared statistically, obtaining a polarization curve of 0.03836 ± 0.001431 (mean $\pm$ s.e.m.) and a power density curve of 0.02889 ± 0.002181. In the single cell of the SFFSB, the areas of hysteresis loops over five cycles were evaluated quantitatively, obtaining a polarization curve of 0.03581 ± 0.0006720 and a power density curve of 0.02307 ± 0.0005538. The average current densities for the single cells of the CASFF at cell's voltage of 0.35 V are 1.310 A/cm^2 and 1.557 A/cm^2, respectively, indicating that the single cell of the SFFSB has higher current density by 18.85% than the single cell of the CASFF. The PEFCs utilized in the experiments featured SFF channels combined with sub-channels and by-passes. Previous studies have shown that the new SFFSB design improves not only the flow consistency of the inner reacting gas and the liquid water behavior but also the current density in the ohmic resistance loss and the mass transport loss regions. Compared to the conventional SFF design, the new SFF design represents a much smaller area surrounded by the hysteresis curve because of a varying electric load. We demonstrate the dynamic behaviors of the single cell with the new SFF that produces additional sub-channels and by-passes with respect to the conventional SFF design.

The maximum power densities for the single cells of the new SFFSB and conventional CASFF are 0.615 W/cm^2 and 0.497 W/cm^2, respectively; both are measured at cell's voltage of 0.47 V. The power density of the SFFSB single cell has higher by 23.74% than that of the CASFF single cell. These results can be explained by the following reasons: rapid diffusion, more uniform of the reactants, improvement of the electrochemical reaction by URC in the activation loss region, optimal water balance inside the cathode channel in the ohmic resistance loss region, increase of membrane conductivity, and increase of mass fraction of the reactants produced at outlet in the mass transport loss region with by-passes.

4.3. Numerical and experimental results of the role of URC in current density distributions

Figure 5 presents the comparison of the current density distributions in the CASFF and SFFSB at the averaged current density of 0.6 A/cm^2. The overall distributions show that the local current density starts decreasing from inlet and continues to decrease until it reaches outlet due to the consumption of the reactants. In the SFFSB, the reactants that are transported into the under-rib region where the improved URC do not react sufficiently and leak out to the adjacent main channel, however at outlet, the remaining reactants increase the current density under the rib area. The current density (I) is proportional to the membrane conductivity as follows [18,27]:

$$I(x,y) = \frac{\sigma_m(x,y)}{t_m}\left(V_{OC} - V_{cell} - \eta(x,y)\right) \quad (1)$$

where $I(x,y)$ is the local current density, $\sigma_m(x,y)$ is the local membrane conductivity, t_m is the membrane thickness, V_{OC} is the cell open circuit voltage, V_{cell} is the cell voltage, and $\eta(x,y)$ is the local overpotential for oxygen reaction.

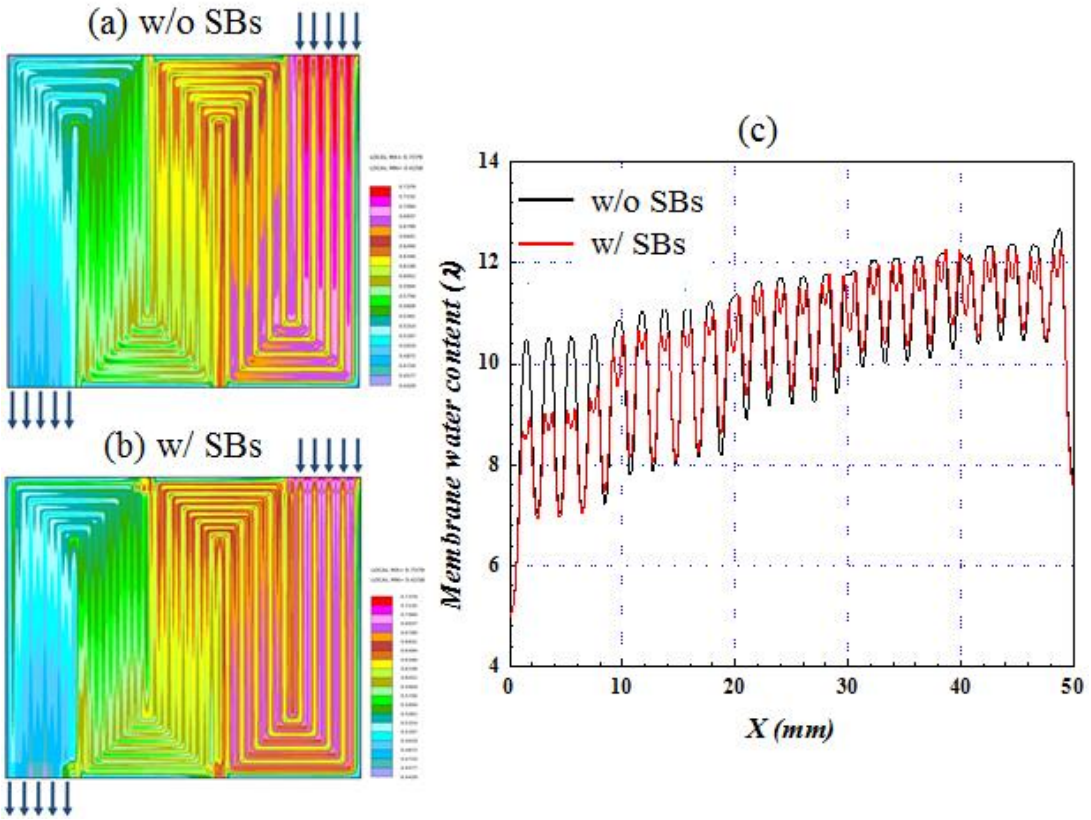

Figure 5. Simulation results of current density distributions in (a) the SFF without SBs are compared with those in (b) the SFF with SBs, and (c) the membrane water contents as the main reason for the discrepancy that the SFF with SBs has a more balanced current density than that of the SFF without SBs at an average current density of 0.6 A/cm^2.

As shown in Fig. 5, the current density of the CASFF (Fig. 5b) has smaller variations between inlet and outlet than that of the SFFSB (Fig. 5a), and figure 5c confirmed by comparing the membrane water contents of CASFF and SFFSB. The membrane water content under the rib areas is higher than that under the main channel areas because almost water produced can be absorbed in the membrane at the cathode under the rib region. The membrane water content increases from inlet toward outlet due to the decrease of total pressure because the membrane water content depends on the water activity as a function of total pressure as follows [18,27]:

$$\begin{aligned}\lambda &= 0.043 + 17.8\alpha_k - 39.85\alpha_k^2 + 36.0\alpha_k^3 \ (0 \le \alpha_k < 1) \\ &= 14.0 + 1.4(\alpha_k - 1) \ \ (1 \le \alpha_k \le 3)\end{aligned} \tag{2}$$

$$\alpha_k = \frac{X_{w,k}P(x,y)}{P_{w,k}^{sat}} \tag{3}$$

where λ is the water content in the membrane, α_k is the activity of water in stream k, $X_{w,k}$ is the mole fraction of water in stream k, $P(x,y)$ is the local pressure, and $P_{w,k}^{sat}$ is the saturated pressure of water in stream k. The membrane water content of the SFFSB has smaller variations between the main channel and the rib than that of the CASFF because URC flows from the main channel to the adjacent rib and

then flows from inlet channel to outlet channel, and liquid water gathers and discharges into the sub-channels. The membrane conductivity is a function of the membrane water content. The uniform current density distribution of the SFFSB makes less mechanical stress on the MEA and eventually longer cell lifetimes. The URC improved the performance related parameters such as activation of CL and water discharge by using the sub-channels.

The *in situ* current density distributions of the single cells of CASFF and SFFSB patterns were measured directly while adjusting the current density from 0.1 A/cm^2 to 1.2 A/cm^2 with 0.1 A/cm^2 steps, as shown in Figures 4, 6 and 7 can be shown the 3-D graph for qualitative comparison and the contour graphs for quantitative comparison of the typical *in situ* current density distribution with the SFF without and with SBs at the averaged current density (I_{avg}) of 0.2 A/cm^2, 0.6 A/cm^2 and 1.0 A/cm^2, typical values in the regions of the activation loss, the ohmic resistance loss, and the mass transport loss, respectively.

The local current density distribution is influenced by mass transfer, such as water management in the overall channel. As shown in both Figs. 6 and 7, current densities in inlet and outlet are lower than those in the other edges. This is because the condensed water produced by the fully humidified reactants in inlet obstructs the electrochemical reaction. The flow directions of the reactants are changed in the other edges and then the electrochemical reaction is activated by URC [3]. This means that the outer wall has a lower current density than the central part. These experimental results can be explained by the relationship among current density, temperature, reactants and product based on the Butler–Volmer equation and Tafel equation [28].

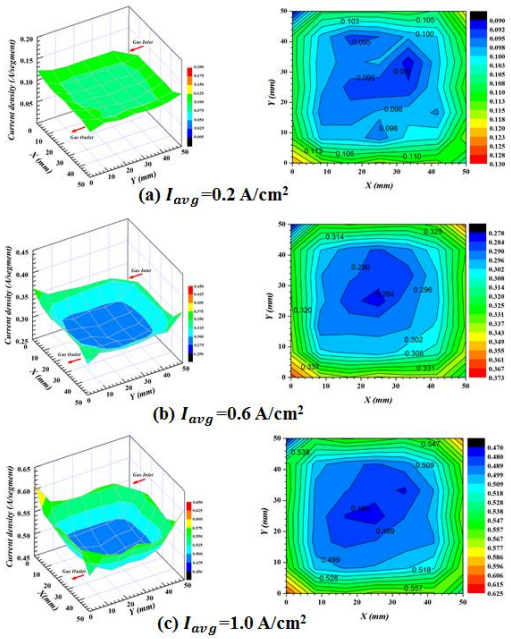

Figure 6. Three-dimensional and contour graphs of the typical *in situ* current density distributions with the single cell of the CASFF were measured directly at the averaged current density (I_{avg}) of 0.2 A/cm^2 of the activation loss region, 0.6 A/cm^2 of the ohmic resistance loss region and 1.0 A/cm^2 of the mass transport loss region.

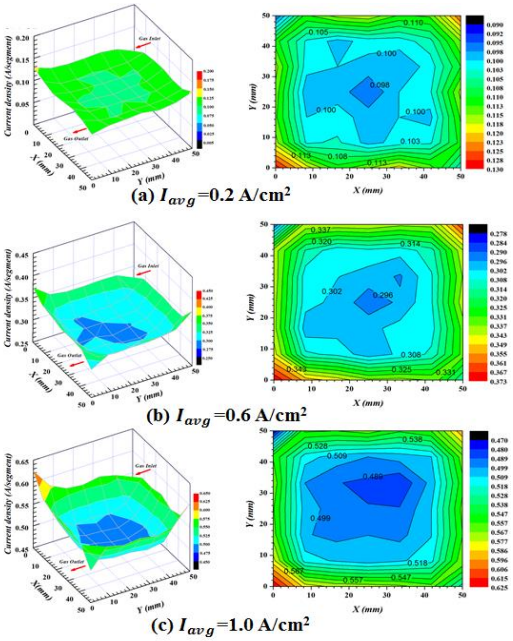

Figure 7. Three-dimensional and contour graphs of the typical *in situ* current density distributions with the single cell of the SFFSB were measured directly at the averaged current density (I_{avg}) of 0.2 A/cm^2 of the activation loss region, 0.6 A/cm^2 of the ohmic resistance loss region and 1.0 A/cm^2 of the mass transport loss region.

The local current density range of 0.092~0.113 in Fig. 6a is slightly lower than that of 0.098~0.113 in Fig. 7a. This is because the reactants have a sufficient H_2 stoichiometric ratio of anode stoichiometric flowrate H_2 1.5: 2.0 cathode stoichiometric flowrate air (Anode: H_2 (g) → $2H^+$+$2e^-$, Cathode: 1/2(O_2+3.76N_2) (g) + 2H + $2e^-$ → H_2O (l), Theoretical stoichiometric flowrate H_2 1.0: 0.5 air), and the activation loss is similar. The local current density range of 0.284~0.337 in Fig. 6b is slightly lower than that of 0.296~0.343 in Fig. 7b. Figures 6b and 7b show the lower current density at the average current density of 0.6 A/cm^2, especially in the central part, and the area of the lower current density with the CASFF become broader than that with the SFFSB. In the case of the SFFSB, the sub-channel changes the flow direction of the URC and the URC flow direction converges to the sub-channel. The improved URC can decrease water flooding at the cathode and increase the electrochemical reaction, thus enhancing both the cell performance and the operating stability. Additionally, the produced water is generated more at the channel than at the rib, cool down the CL and reduce the electrochemical reaction. Therefore, the CASFF of smaller rib width shows a lower current density at the central part than the SFFSB. These results means that the current density distribution usually shows a greater difference in the center region with more active flow as in the outer regions of the flow-field. Specifically, the corner area, except inlet and outlet of the flow-field, has a high current density. This is caused by the increasing pressure that is a result of the flow direction change of the reactants. In the center region, the flow consistency is improved by URC by displaying a consistent current density, and it is perfectly clear that there is a difference between the local current density in the range of 0.480~0.557 in Fig. 6c and 0.489~0.567 in Fig. 7c at the averaged current density of 1.0 A/cm^2.

PEFC's polarization performance was influenced by the inner behavior and was especially

sensitive to the behavior of liquid water in the electrochemical reaction. The effect of the liquid water inside the flow-field increased the water content of the MEA by migrating through main channel from the anode to the cathode. Furthermore, the liquid water cooled down the heat produced by the electrochemical reaction. The new SFFSB improved the flow consistency of the inner reaction gas and the liquid water behavior, and the current density distribution keeps uniform in the regions of activation loss, ohmic resistance loss, and mass transport loss. Compared with the CASFF, the effects of the new SFFSB are rapid diffusion, more uniform of the reactants, improvement of the electrochemical reaction by URC in the activation loss region, optimal water balance inside the cathode channel in the ohmic resistance loss region, increase of membrane conductivity, and increase of mass fraction of the reactants produced at outlet in the mass transport loss region with by-passes.

5. CONCLUSIONS

This study presents the experimental and numerical results with single cells of a new flow-field, stimulating URC with additional sub-channels and by-passes to a conventional flow-field with 5-passes and 4-turns on an active area of 25 cm^2. To characterize the role of under-rib convection for PEFC polarization performance, the performance-related parameters of the *in situ* reactants and liquid water flows, hysteresis effects and current density distributions of the new SFFSB were compared experimentally and numerically with those of a CASFF. In the CASFF where URC is not generated by the flow-field pattern of reactants inside a PEFC, reactants moved from the entrance toward the exit through the lower part of the rib due to the pressure difference. In the new SFFSB where the sub-channels and by-passes are added between the main channels, the URC flow-field pattern changes the main channels toward the sub-channels, then realizes more effective utilization of electrocatalysts by increasing reactants concentration, facilitating liquid water removal in those regions and producing uniform current density distribution. The flow-field pattern that activates the internal mass transfer mechanism of PEFC is able to improve its performance from a mechanical engineering perspective.

Compared to the CASFF design, the new SFFSB design represents a much smaller area surrounded by the hysteresis curve due to a varying electric load. The hysteresis effects of PEFCs were investigated between the SFF without and with SBs designs. In the single cell of the CASFF, the areas of hysteresis loops over five cycles were compared quantitatively, obtaining a polarization curve of 0.03836 ± 0.001431 (mean $\pm$ s.e.m.) and a power density curve of 0.02889 ± 0.002181. In the single cell of the new SFFSB, the areas of hysteresis loops over five cycles were evaluated quantitatively, obtaining a polarization curve of 0.03581 ± 0.0006720 and a power density curve of 0.02307 ± 0.0005538. When the membrane of a PEFC is fully hydrated, the water is balanced within the MEA. A larger void volume in the diffusion layer is most likely to be occupied by liquid water. The PEFC can run at a higher current density with a small degree of gas diffusion if the generated water is carried out of the PEFC by the reacting gas. Compared to the CASFF design, the new SFF design represents a much smaller area surrounded by the hysteresis curve because of a varying electric load. We demonstrate the dynamic behaviors of the single cell with the new SFF that produces additional sub-channels and by-passes with respect to the conventional SFF design.

In the experimental PEFC polarization performance evaluation, the average current density of the new SFFSB, 1.557 A/cm^2, was increased by 18.85% compared to that of the CASFF, 1.310 A/cm^2, at cell's voltage of 0.35 V, and the maximum power densities of the SFFs with and without SBs were 0.615 and 0.497 W/cm^2 at cell's voltage of 0.47 V, respectively, yielding an improvement of 23.74% in the new SFFSB. The current density distribution provided the PEFC polarization performance improved by URC with the new SFFSB. The URC stimulated by the new SFFSB realizes more effective utilization of electrocatalysts by increasing reactants concentration and facilitating liquid water removal into URC regions. the effects of the new SFFSB are rapid diffusion, more uniform of the reactants, improvement of the electrochemical reaction by URC in the activation loss region, optimal water balance inside the cathode channel in the ohmic resistance loss region, increase of membrane conductivity, and increase of mass fraction of the reactants produced at outlet in the mass transport loss region with by-passes at outlet in the mass transport loss region with by-passes. The URC generated by the new SFFSB design will play an important role in improving PEFC polarization performance, as well as increasing the fuel cell lifetime.

ACKNOWLEDGEMENTS
This work was supported by the 2018 Inje University research grant.

References

1. A. L. Rangel-Cárdenas, G. J. M. Koper, *Materials (Basel)*, 10 (2017) 576.
2. V. N. Duy, K. Kim, J. Lee, J. Ahn, S. Park, T. Kim, H. M. Kim, *Int. J. Electrochem. Sci*., 10 (2015) 5842.
3. K. S. Choi, B. G. Kim, K. Park, H. M. Kim, *Fuel Cells*, 12 (2012) 908.
4. C. Wang, Q. Zhang, S. Shen. X. Yan, F. Zhu, X. Cheng, J. Zhang, *Sci. Rep.*, 7 (2017) 43447.
5. V. Lonescu, *Procedia Manuf.*, 22 (2018) 642.
6. N. D. Vinh, H. M. Kim, *energies*, 9 (2016) 844.
7. Y. H. Lai, K. M. Rahmoelle, J. H. Hurst, R. S. Kukreja, M. Atwan, A. J. Maslyn, C.S. Gittleman. McAuley, *J. Electrochem. Soc.*, 165 (2018) F3217.
8. T. Bednarek, G. Tsotridis, *J. Power Sources*, 343 (2017) 550.
9. S. Praveenkumar, S. Muruganantham, and M. Muthukumar, *IJSRIT*, 13 (2015) 152.
10. D. Zhang, Q. Cai, S. Gu, *Electrochem. Acta*, 262 (2018) 282.
11. A. Iranzo, J. Biesdorf, M. Cochet, A. Salva, P. Boillat, F. Rosa, *Fuel Cells*, 16 (2016) 777.
12. K. S. Choi, H. M. Kim, and S. M. Moon, *Electrochem Commun*., 13 (2011) 1387.
13. K. S. Choi, B.G. Kim, K. Park, and H. M. Kim, *Comput. Fluids*, 69 (2012) 81.
14. B. Lee, K. Park, and H. M. Kim, *Int. J. Electrochem. Sci*., 8 (2013) 219.
15. K. Park, H.M. Kim, K. S. Choi, *Fuel Cells*, 13 (2013) 927.
16. K. S. Choi, J. W. Ahn, J. K. Lee, D. V. Nguyen, H. M. Kim, K.W. Park, and G. Y. Hwang, *IEEE Trans. Energy Convers*., 29 (2014) 727.
17. N. D. Vinh, J. Lee, K. Kim, J. Ahn, S. Park, T. Kim, H. M. Kim, *J. Power Sources*, 293 (2015) 447.
18. K. S. Choi, H. M. Kim and S. M. Moon, *Int. J. Hydrogen Energy*, 36 (2011) 1613.
19. K. Park, J. Lee, H.-M. Kim, K.-S. Choi, G. Hwang, *Sci. Rep.*, 4 (2014) 4592.
20. R. Bove, T. Malkow, A. Saturnio, G. Tsotridis, *J.* Power *Sources*, 180 (2008) 452.
21. R. Kraume, Current Scan LIN, Rev. 3.2, S++ Simulation Services (2008) Germany.
22. D. G. Strickland, S. Litster, J. G. Santiago, *J. Power Sources*, 174 (2007) 272.
23. C. M. Bautista-Rodríguez, J. A. Bañuelos, A. de la Luz-Pedro, M. M. Santoyo, R. R. Lindeke, *Int.*

J. Electrochem. Sci., 13 (2018) 4223.
24. T. Reshetenko, A. Kulikovsky, *J. Electrochem. Soc*., 163 (2016) F1100.
25. T. Reshetenko, A. Kulikovsky, *J. Electrochem. Soc*., 164 (2017) F1633.
26. B. Ibrahimoglu, M. Z. Yilmazoglu, *Fuel Cells*, 17 (2017) 786.
27. S. Shimpalee, J. W. Van Zee, *Int J Hydrogen Energy*, 32 (2007) 842.
28. A. R. Kucernak, C. Zalitis, *J. Phys. Chem. Lett.*, 120 (2016) 10721.